RESEARCH ARTICLE

Visible Light-Conjugation with Triazolinediones as a Route to Degradable Poly(ethylene glycol)-Lipids for mRNA Lipid Nanoparticle Formulation

Bianka Golba[a], Matthieu Soete[b], Zifu Zhong[a], Niek Sanders[c], Filip E. Du Prez[b], Hannes A. Houck*[b] and Bruno G. De Geest*[a]

[a] B. Golba, Dr. Z. Zhong and Prof. Dr. B. G. De Geest
Department of Pharmaceutics,
Ghent University,
Ottergemsesteenweg 460, 9000 Ghent (Belgium).
E-mail: br.degeest@ugent.be

[b] M. Soete, Prof. Dr. F. E. Du Prez, Dr. Hannes A. Houck
Polymer Chemistry Research group
Centre of Macromolecular Chemistry (CMaC)
Department of Organic and Macromolecular Chemistry
Ghent University
Krijgslaan 281, S4-bis, 9000 Ghent (Belgium).
E-mail: hannes.houck@warwick.ac.uk

[c] Prof. Dr. Niek Sanders
Department of Veterinary and Biosciences
Ghent University
Heidestraat 19, 9820 Merelbeke (Belgium).

Supporting information for this article is given via a link at the end of the document.

Abstract: Polyethylene glycol (PEG) is considered as the gold standard for colloidal stabilization of nanomedicines, yet PEG is non-degradable and lacks functionality on the backbone. Herein, we introduce concomitantly PEG backbone functionality and degradability via a one-step modification with 1,2,4-triazoline-3,5-diones (TAD) under green light. The TAD-PEG conjugates are degradable in aqueous medium under physiological conditions, with the rate of hydrolysis depending on pH and temperature. Subsequently, a PEG-lipid is modified with TAD-derivatives and successfully used for messenger RNA (mRNA) lipid nanoparticle (LNP) delivery, thereby improving mRNA transfection efficiency on multiple cell cultures *in vitro*. *In vivo*, in mice, mRNA LNP formulation exhibited a similar tissue distribution as common LNPs, with a slight decrease in transfection efficiency. Our findings pave the road towards the design of degradable, backbone-functionalized PEG for applications in nanomedicine and beyond.

Introduction

mRNA as a drug molecule holds immense potential for a wide range of therapeutic applications, including vaccination, immunotherapy, protein replacement therapy and genome editing.[1,2] mRNA is inactive in unformulated form due to rapid degradation in the extracellular environment and the inability to cross the phospholipid cell membrane and reach its molecular target in the cytoplasm.[1,3] Encapsulation of mRNA in LNPs exactly addresses these hurdles. LNPs protect mRNA from degradation, facilitate endocytosis and mediate delivery of intact mRNA into the cytoplasm of actively phagocyting cells.[4,5] LNP formulations of small interfering RNA (siRNA; Onpattro) are approved for the treatment of polyneuropathy while the mRNA-LNP drug products Comirnaty and Spikevax have reached the global market as vaccines against Covid-19.[6] These LNP formulations comprise 4 lipid components: (1) an ionizable lipid for electrostatic complexation of mRNA and rupturing of the endosomal membrane, (2) a phospholipid for additional stabilization of the LNP and enhancing endosomal escape, (3) cholesterol to enhance fluidity and LNP stability, and (4) a poly(ethylene glycol)-lipid conjugate (PEG-lipid) for colloidal stabilization.[7,8]

PEG, is a hydrophilic polymer that is used in many clinically-approved drug formulations and is known to prolong blood circulation time and reduce opsonization of nanomedicines.[9] Despite the therapeutic benefits, administration of PEGylated proteins[10,11] and PEGylated nanoparticles[12–15] can generate anti-PEG antibodies in the host which is also reported in case of Covid-19 vaccines[16]. Anti-PEG antibodies result in accelerated blood clearance of the drug and, thereby, reduce therapeutic efficacy. Long term accumulation of PEG in the body has also fostered the quest for PEG alternatives[17,18] and strategies that reduce the exposure to PEG. The latter has been attempted by using PEG conjugates with

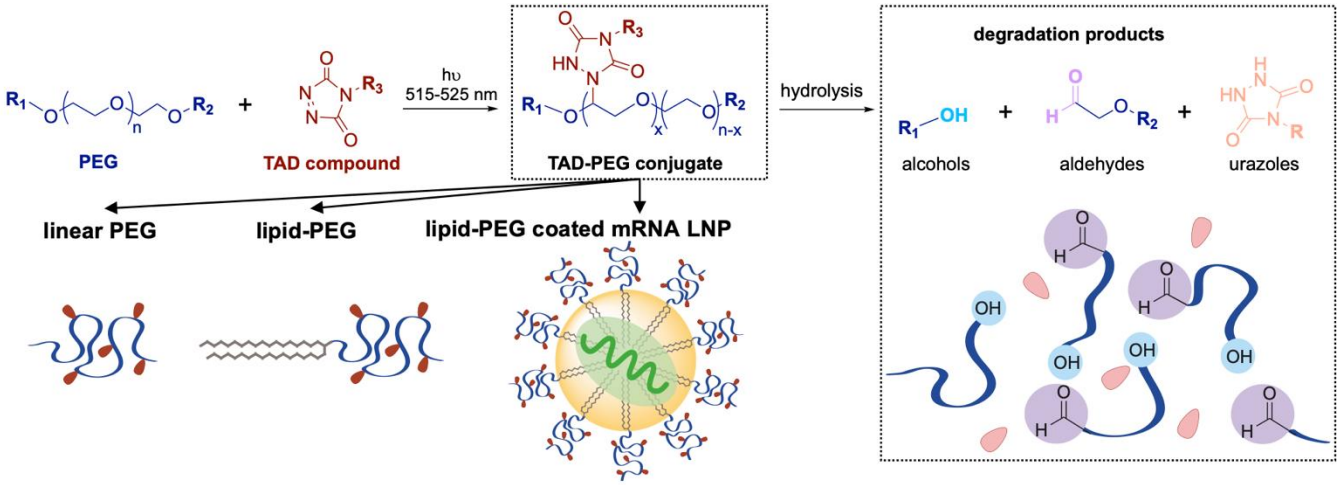

Figure 1. Schematic overview of the PEG photo-modification strategy with 1,2,4-triazoline-3,5-dione (TAD), yielding hydrolysable TAD-PEG conjugates that degrade in aqueous media.

shorter half-life times,[19] designing triggered de-PEGylation strategies,[20,21] or by conjugating targeting or imaging ligands to PEG [22,23].

The polyether backbone of PEG is non-degradable under common physiological conditions and lacks functional groups for chemical derivatization. Introduction of functional groups onto the PEG backbone is relatively cumbersome and requires the use of functional epoxides during the ring-opening polymerization of ethylene oxide.[24–26] TADs provide an interesting alternative to introduce functional groups along the PEG backbone (**Figure 1**). Under UV or visible light irradiation (λ = 320 – 600 nm), the cyclic azo-compound readily undergoes an α-addition to ethers in a formal photoreduction, involving the formation of a urazolyl radical intermediate and a hydrogen abstraction process.[27,28] The thus formed α-urazolyl ethers contain hemiaminal ether type bonds that can be hydrolyzed in an aqueous environment.[27] Interestingly, TAD-modification rendered the PEG backbone prone to hydrolytic cleavage under physiologically relevant conditions, as demonstrated for a water-degradable organogel under neutral conditions at 37 °C.[27]

In this work, we hypothesized that degradability of the PEG backbone, resulting from TAD photo-modification, holds potential to mitigate concerns regarding long term accumulation of PEGylated substrates in the body, particularly of high molecular weight PEG.[29] Therefore, we developed a conjugation strategy to modify biomedically-relevant PEGs with TADs to introduce both functional groups and degradability along the polyether backbone in a single, straightforward step. Specifically, we demonstrate that the hydrolysis rate of TAD-PEG conjugates depends on pH and temperature of the aqueous environment. We applied these insights to a commercial PEG-lipid that is used in clinically approved mRNA LNP formulations. We show for different model TAD-compounds concomitant introduction of degradability and functionality onto the PEG backbone. The effect of TAD-conjugation on the capacity of the TAD-PEG-lipid to provide colloidal stabilization to mRNA-LNP was investigated and toxicity on *in vitro* cell cultures was studied. Moreover, the ability of TAD-PEG-lipid formulated mRNA-LNP to exhibit increased transfection efficiency *in vitro* was assessed. Finally, *in vivo* experiments, in mice, were carried out with the TAD-PEG-lipid formulated mRNA-LNP to visualize tissue distribution and transfection efficacy compared to common LNP.

Results and Discussion

Temperature- and pH-dependent Degradation Kinetics of TAD-PEG in Aqueous Medium

TAD-ether adducts have been observed to undergo hydrolysis, but a more detailed screening of the degradation kinetics as a function of both temperature and pH has not yet been reported. We selected a 2 kDa PEG as a model substrate owing to its similarity in molecular weight to the PEG-lipid derivatives used in clinically approved siRNA and mRNA LNP formulations. Prior to TAD-conjugation, the hydroxyl end groups of bis-hydroxyl-PEG were reacted with *tert*-butyl isocyanate to avoid possible side reactions between the hydroxyl groups and the TAD reagents. Moreover, the thus incorporated *tert*-butyl polymer end groups provide an internal standard, enabling quantification of the average number of covalently bound TAD units per polymer chain by ^{1}H-NMR analysis.[27] For simplicity, the obtained *tert*-butyl end capped PEG will be further referred to as PEG in this paper.

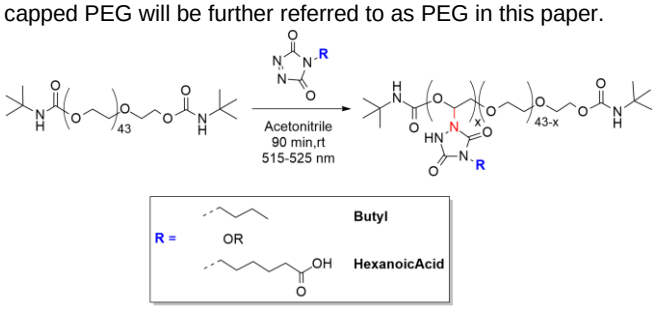

Scheme 1. Conjugation of PEG with ^{Butyl}TAD or ^{HexanoicAcid}TAD under green light irradiation (λ = 515-525 nm, 64 mW cm^{-2}).

Thus, PEG conjugates with 4-*n*-butyl-TAD and 6-(3,5-dioxo-4H-1,2,4-triazol-4-yl)hexanoic acid, further referred to as ^{Butyl}TAD and ^{HexanoicAcid}TAD, respectively, were obtained under green light irradiation (λ = 515-525 nm, 64 mW cm^{-2}) for 90 min in acetonitrile

(**Scheme 1**). The degree of substituted polyether repeating units can be tuned up to 30% by increasing the initial amount of TAD equivalents.[27] In this work, we targeted a degree of substitution (DS), defined as the average number of ether repeating units in the PEG backbone modified with TADs, of 4.4, which corresponds to a 10% degree of functionalization. The TAD-PEG conjugates were isolated by removal of the solvent under vacuum and submitted to ^{1}H-NMR analysis (**Figure S2 and S3**), indicating a DS of 3.2 for ^{HexanoicAcid}TAD-PEG and 4.2 for ^{Butyl}TAD-PEG.

Following the straightforward synthesis of the two TAD-PEG conjugates, SEC analysis was used to investigate the hydrolysis of the embedded hemiaminal ether linkages as a function of time in different aqueous buffers (i.e., pH 5.5, 7.4 and 9) and temperature (i.e., 25°C and 40°C) values. These pH values were selected as a mimic of the endosomal (pH 5.5) and neutral physiological pH (7.4). A pH value of 9 was selected as a mild alkaline pH value. Temperature values were selected as an approximation of room and physiological temperature. TAD conjugation is a random process and can take place at any α–carbon position along the polyether chain. Hence, oligomeric degradation products with varying molecular weights are expected to be formed.[27] Indeed, the SEC elugrams of the TAD-PEG conjugates in **Figure 2** show peak broadening towards longer elution times, and hence lower molecular weights, occurring over time. In contrast, no hydrolysis was observed for the native, unmodified PEG (**Figure S4**). Over a time course of 2 weeks, extensive TAD-PEG degradation was observed at ambient temperature in both pH 5.5 and 7.4 buffers.

TAD can be considered as a cyclic analogue of diethyl azodicarboxylate (DEAD). The latter was reported to form hemiaminal-type linkages with ethers being susceptible to hydrolysis in water under neutral conditions forming diethyl hydrazo-dicarboxylate, alcohol and carbonyl compounds.[30–33] Hence, analogous degradation products are expected to be formed following the hydrolysis of hemiaminal-type linkages present in the TAD-PEG adducts. ^{1}H-NMR analysis of ^{Butyl}TAD-PEG in aqueous medium supported this hypothesis by showing resonance peaks that could be attributed to aldehyde, alcohol and urazole moieties (**Figure S5**). A plausible mechanism for the hydrolysis of TAD-PEG adducts likely proceeds through a zwitterionic urazole intermediate stabilized via electron delocalization within the ring structure of the adduct (**Scheme 2**). A neutral urazole moiety can hence be eliminated from the polymer backbone with the formation of an oxonium ether. The latter can subsequently hydrolyze, forming aldehyde and alcohol products via the intermediate formation of a hemi-acetal.

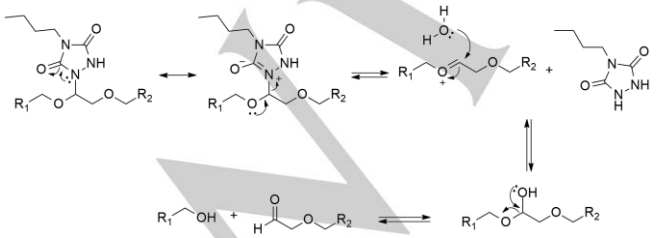

Scheme 2. Proposed plausible mechanism for the hydrolysis of TAD-PEG conjugates, illustrated for ^{Butyl}TAD-PEG.

During the hydrolysis studies, polymer degradation was observed to proceed almost equally efficient under both neutral (pH 7.4) and acidic (pH 5.5) conditions, hence enabling PEG backbone degradation to be induced under milder conditions. This rather unexpected prominent hydrolysis at pH 7.4 can be attributed to the increased leaving group capacity of the 1,4-urazole adduct. In contrast to common acetal or hemiaminal ether

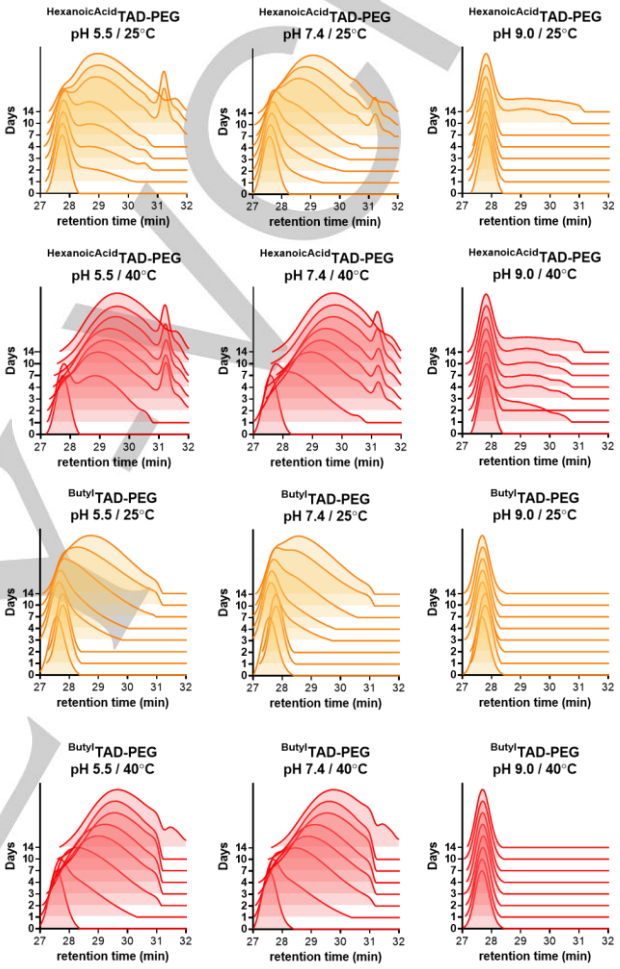

Figure 2. SEC elugrams of ^{HexanoicAcid}TAD-PEG and ^{Butyl}TAD-PEG exposed to aqueous buffers of different pH and temperature as a function of time. (solvent: THF, standards: polystyrene).

hydrolysis that requires initial protonation of the leaving group for the reaction to proceed,[34] the decreased pKa of a urazole moiety (~5-6[35,36]) allows it to be expelled even in the absence of a (strong) acid. Consequently, oxonium intermediates can be readily formed under milder conditions, thereby initiating backbone scission along the statistically modified polymer. Interestingly, only little degradation (<5% after 14 days) was observed at pH 9 (25°C). We postulate that this pH dependency arises from the fact that, in an alkaline environment, the free N-H of the TAD-PEG adduct will be predominantly deprotonated[37] and thereby prevent urazole elimination. Even though minor degradation could be seen for the ^{HexanoicAcid}TAD-PEG at elevated temperatures (40°C, pH 9), these hydrolysis experiments enabled

the pH to serve as a straightforward trigger for the on-demand degradation of modified PEGs. Degradation of both TAD-PEGs was clearly accelerated at 40°C. Moreover, ^{HexanoicAcid}TAD-PEG showed faster hydrolysis than ^{Butyl}TAD-PEG during all experiments, an observation that can likely be ascribed to either the more hydrophilic environment around the degradation sites or to a catalytic effect arising from the incorporated carboxylic acid moieties.

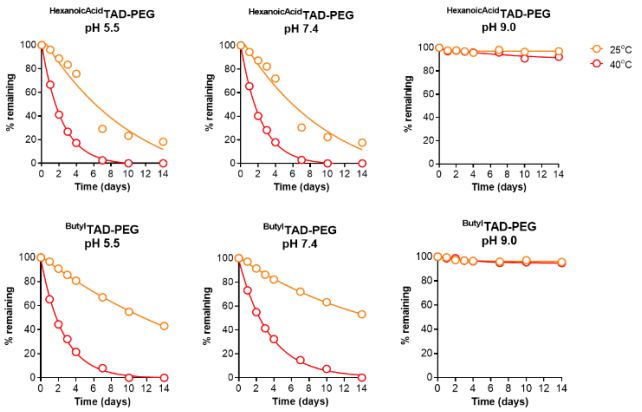

Figure 3. Hydrolysis of ^{HexanoicAcid}TAD-PEG and ^{Butyl}TAD-PEG monitored by ^{1}H-NMR spectroscopy. The '% remaining' is here defined as the fraction of non-hydrolyzed TAD conjugate relative to the initial amount of TAD conjugate, determined via integration of the α-urazolyl CH proton.

In addition to SEC, ^{1}H-NMR analysis of the α-CH proton signals corresponding to the formed α-urazolyl ether products (*cfr.* **Figure S2-S3**) was used to gain quantitative insights into the hydrolysis kinetics of the TAD-PEG conjugates. Similar experimental conditions as for SEC analysis (*vide supra*) were selected. Data obtained by ^{1}H-NMR analysis (**Figure 3**) were fully consistent with SEC analysis data, i.e. hydrolysis of ^{HexanoicAcid}TAD-PEG was faster than ^{Butyl}TAD-PEG at pH 5.5 and 7.4, whereas at pH 9 minimal hydrolysis was observed. At higher temperature, hydrolytic degradation proceeded faster, while the native, unmodified PEG remained invariant over 14 days in aqueous medium at pH 5.5 and 40°C (**Figure S6**). **Table 1** summarizes the calculated half-life times ($t_{1/2}$) for the hydrolysis of ^{Butyl}TAD-PEG and ^{HexanoicAcid}TAD-PEG assuming apparent 1st order kinetics. Notably, fitting the experimental data to a linear regression model yielded a reliable estimation of the degradation half-life times only at conditions where significant hydrolysis was detectable by ^{1}H-NMR. Hence, in the case of the observed very slow degradation at pH 9, linear regression analysis was not possible (**Table 1** and **Figures S7-12**).

Table 1. Calculated half-life times ($t_{1/2}$) and R^2 values corresponding to the linear regression fit for the hydrolysis of ^{Butyl}TAD-PEG and ^{HexanoicAcid}TAD-PEG at different pH and temperatures (T).

	T	$t_{1/2}$ (days) @ pH7.4	R^2 @ pH7.4	$t_{1/2}$ (days) @ pH5.5	R^2 @ pH5.5
^{Butyl}TAD-PEG	40°C	3.8	0.998	2.8	0.998
	25°C	21.8	0.998	16.3	0.999
^{HexanoicAcid}TAD-PEG	40°C	2.0	0.990	1.9	0.989
	25°C	7.0	0.946	7.1	0.933

Synthesis and Characterization of Degradable TAD-PEG-lipids

1,2-dimyristoyl-rac-glycero-3-methoxypolyethylene glycol-2000 (PEG-DMG, 2 kDa PEG), used in Moderna's Spikevax mRNA-LNP formulation[7], was conjugated with ^{HexanoicAcid}TAD and ^{Butyl}TAD, respectively, in a similar fashion as PEG (*vide supra*) (**Scheme 3**). ^{1}H-NMR analysis (**Figure S13 and S14**) indicated successful covalent polymer conjugation with an experimental DS of 3.8 for ^{HexanoicAcid}TAD-PEG-DMG and 3.9 for ^{Butyl}TAD-PEG-DMG. Notably, attempts to verify DS of TAD-PEG-DMG conjugates by electrospray ionization (ESI) and matrix-assisted laser desorption/ionization-time of flight (MALDI-TOF) mass spectrometry (MS) were unsuccessful due to overlapping charge distributions (**Figure S25**) or insufficient ionization (data not shown), respectively. We then functionalized diethyl ether, as a small molecule model compound, with ^{Butyl}TAD in a similar fashion (*vide supra*) to monitor hydrolysis (**Figure S26**). Investigation of the hydrolysis products via ESI-MS indicated formation of free urazole (**Figure S27**) while this technique was not successful for the detection of the remaining hydrolysis products.

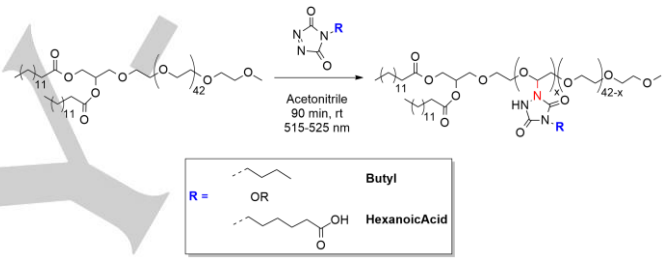

Scheme 3. Synthesis of ^{HexanoicAcid}TAD-PEG-DMG and ^{Butyl}TAD-PEG-DMG.

Following modification, the hydrolysis of the TAD-PEG-DMG conjugates in aqueous pH 5.5 and pH 7.4 buffers and at temperatures of 4, 25 and 37 °C, mimicking cold, ambient storage and physiological temperatures, was investigated by ^{1}H NMR spectroscopy. The rate of hydrolysis appeared slightly faster at a pH of 5.5 compared to pH 7.4 and increased with temperature (**Figure 4**). Hydrolysis was minimal at 4 °C, suggesting the suitability of TAD-PEG-DMG LNP formulations for cold storage. On the other hand, ^{HexanoicAcid}TAD-PEG-DMG hydrolysis appeared to be faster than the one of ^{Butyl}TAD-PEG-DMG. Hence, the influence of temperature, pH and nature of TAD-substitution showed a similar trend for the TAD-PEG-DMG conjugates as for the TAD-PEG model substrates. **Table 2** summarizes the calculated $t_{1/2}$ for the hydrolysis of ^{Butyl}TAD-PEG-DMG and ^{HexanoicAcid}TAD-PEG-DMG assuming apparent 1st order kinetics. Also in this case, fitting of the experimental data to a linear regression model yielded a reliable estimation of the degradation half-life times only at conditions where significant hydrolysis was detectable by ^{1}H-NMR. Hence, in the case of the observed very slow degradation at 4 °C, linear regression analysis was not possible (**Table 2** and **Figures S16-19**).

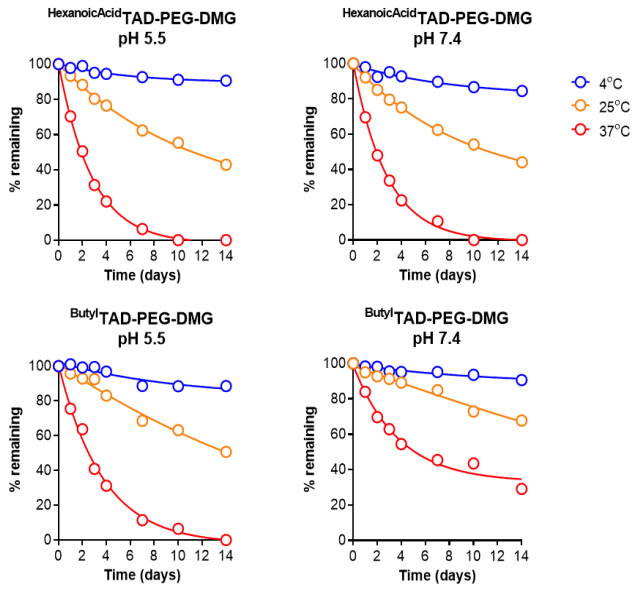

Figure 4. Hydrolysis of ^{HexanoicAcid}TAD-PEG-DMG and ^{Butyl}TAD-PEG-DMG monitored by ^{1}H-NMR spectroscopy. The '% remaining' is here defined as the fraction of non-hydrolyzed TAD conjugate relative to the initial amount of TAD conjugate, determined via integration of the α-urazolyl CH proton.

Table 2. Calculated half-life times ($t_{1/2}$) and R^2 values corresponding to the linear regression fit for the hydrolysis of ^{Butyl}TAD-PEG-DMG and ^{HexanoicAcid}TAD-PEG-DMG at different pH and temperatures (T).

	T	$t_{1/2}$ (days) @ pH7.4	R^2 @ pH7.4	$t_{1/2}$ (days) @ pH5.5	R^2 @ pH5.5
^{Butyl}TAD-PEG-DMG	37°C	12.7	0.932	3.5	0.990
	25°C	36.2	0.977	20.1	0.985
^{HexanoicAcid}TAD-PEG-DMG	37°C	3.1	0.990	2.5	0.998
	25°C	17.4	0.993	16.8	0.995

Formulation of mRNA in LNP with TAD-PEG-lipids

To assess the applicability of the TAD-PEG-DMG conjugates for mRNA LNP formulation, mRNA encoding for enhanced green fluorescent protein (eGFP) was formulated into LNPs containing PEG-DMG, ^{HexanoicAcid}TAD-PEG-DMG and ^{Buty}TAD-PEG-DMG, respectively. LNPs were prepared by solvent displacement, adding a buffered (pH 4.0) aqueous solution containing mRNA to a lipid mixture in ethanol under vigorous stirring. The lipid mixture comprised ALC-0315 as an ionizable lipid (used in BioNTech/Pfizer Comirnaty mRNA-LNP formulation), 1,2-distearoyl-sn-glycero-3-phosphocholine (DSPC) as a phospholipid, cholesterol and TAD-PEG-DMG at a 50/10/38.5/1.5 molar ratio[38]. LNP formulations were dialyzed against deionized water to remove ethanol. Biophysical characterization of the obtained mRNA LNP formulations was done by dynamic light scattering (DLS) to determine their size, electrophoretic mobility for the zeta-potential, RiboGreen RNA assay for mRNA encapsulation efficiency and 2-(*p*-toluidino)-6-napthalenesulfonic acid (TNS) assay for measuring the apparent pK_a. The obtained results are summarized in **Table 3**.

DLS analysis indicated the formation of nanoparticles with a low polydispersity index (PDI) for all LNPs. ^{Butyl}TAD-PEG-DMG LNP had a slightly larger diameter compared to PEG-DMG LNP. ^{HexanoicAcid}TAD-PEG-DMG LNPs were much larger, having a diameter of 226 ± 6 nm, which is outside the optimal range (~100 nm) for successful *in vivo* application.[39] The size difference observed between the two TAD-PEG-DMG LNPs may be attributed to various factors. Hydrophilic (urazole and carboxylic acid) and hydrophobic (alkyl chains) moieties were incorporated into the PEG backbone and are presumably located on the LNP surface as evidenced by their colloidal stability in aqueous media. However, it is also possible that the TAD-modified PEG interacts with other LNP components, through electrostatic interactions, hydrogen bonding, and hydrophobic interactions, and the interplay of these interactions likely determines the final LNP size. DMG-PEG LNP had a close to neutral zeta-potential in buffers at pH 5.5 and 7.4, while TAD-PEG-DMG LNP had strongly negative zeta-potential at pH 7.4 and a more mildly negative zeta potential at pH 5.5. We attribute these negative values to the acidic N*H* protons of the urazole with a reported $pK_a \approx 5$.[35] Moreover, the carboxylic acid moieties introduced along the polymer backbone of ^{HexanoicAcid}TAD-PEG-DMG also likely contributed to the negative zeta-potential values although only a subtle difference in zeta-potential between both TAD-PEG-DMG LNPs was observed. Nonetheless, TAD modification reduced the apparent pK_a of ^{HexanoicAcid}TAD-PEG-DMG LNP but not of ^{Butyl}TAD-PEG-DMG LNP. Encapsulation efficiency of mRNA in TAD-PEG-DMG LNP was similar to PEG-DMG LNP, suggesting that anionic charges from the TAD moieties did not hinder the electrostatic complexation between mRNA and the ionizable lipid. We tested the stability of the LNP by incubating them at pH 5.5 and 7.4, and at temperatures of 25 and 37 °C. DLS analysis indicated that all LNP formulations maintained their colloidal stability as no change in size or light scattering intensity was observed (**Figure S20**). Thus, the extent of TAD-PEG-DMG degradation that occurred within this time frame did not lead to an apparent colloidal destabilization of the LNPs.

In Vitro mRNA Transfection Efficiency of TAD-PEG-lipid LNP

mRNA LNP transfection was tested *in vitro* on 4 different cell lines: murine colon adenocarcinoma (MC38), murine colorectal carcinoma (CT26), murine dendritic cells (DC2.4) and human T lymphocytes (Jurkat). mRNA encoding for eGFP, as a reporter protein, was used in combination with Cy5-1,2-distearoyl-sn-glycero-3-phosphoethanolamine (DSPE-Cy5) labeled LNP for concomitant flow cytometry analysis of eGFP expression and cellular uptake of LNP. ^{Butyl}TAD-PEG-DMG LNP exhibited, on all cell lines, a higher transfection efficiency than PEG-DMG and ^{HexanoicAcid}TAD-PEG-DMG LNP (**Figure 5**), at low (50 ng mRNA/well) and high (200 ng mRNA/well) mRNA dose.
The increased transfection efficiency of TAD-PEG-DMG LNP was not attributed to higher cellular uptake of the LNPs. Uptake of ^{Butyl}TAD-PEG-DMG LNP was on par with PEG-DMG LNP, based

Table 3. Biophysical properties of formulated LNPs with unmodified, ^{Butyl}TAD- and ^{HexanoicAcid}TAD- modified PEG-DMG.

	Diameter[1] (nm)	PDI	Zeta potential[2] @ pH 7.4 (mV)	Zeta-potential[2] @ pH 5.5 (mV)	mRNA encapsulation efficiency (%)[4]	Apparent pKa[5]
PEG-DMG	116 ± 2	0.136	-5 ± 5	3 ± 19	44 ± 2	6.6
^{Butyl}TAD-PEG-DMG	144 ± 2	0.094	-32 ± 8	-7 ± 6	56 ± 1	6.6
^{HexanoicAcid}TAD-PEG-DMG	226 ± 6	0.110	-35 ± 8	-11 ± 11	51 ± 5	6.3

[1]Z-average diameter measured by DLS. [2]Measured in 20 mM HEPES buffer, pH 7.4. [3]Measured in 20 mM acetate buffer, pH 5.5.[40,41] [4]Measured by RiboGreen RNA assay, calculated as the fraction of encapsulated mRNA in LNP to total amount of mRNA used in the formulation. [5]Measured by TNS assay, calculated as the pH corresponding to 50% LNP protonation. Data represents the average of 3 experimental repeats ± standard deviation.

on flow cytometry of the cellular Cy5 fluorescence. Uptake of ^{HexanoicAcid}TAD-PEG-DMG LNP was significantly lower. Whereas this could be attributed to a difference in surface chemistry (i.e. deprotonated carboxylic acid moieties could contribute to electrostatic repulsion with the negatively charged cell surface), the almost two-fold larger diameter of ^{HexanoicAcid}TAD-PEG-DMG LNP might also have a major impact on the observed differences in cellular uptake. Notably, TAD-conjugation did not have a negative impact on the viability of cells treated with LNPs (**Figure S21**). Confocal microscopy of cells treated with fluorescently (*i.e.*, PE-Cy5) labelled LNP revealed a dotted pattern (**Figure S28**), indicative of LNP located in endosomal vesicles. Improving endosomal escape remains a critical challenge in RNA delivery, with literature reports suggesting less than 2% of the encapsulated RNA escaping the endosome.[42] To assess whether TAD-conjugation of PEG-DMG would alter the endosomolytic properties of the LNP, we tested hemolysis at pH 5.5 as a mimic for the endosomal pH. All LNPs induced a similar percentage of hemolysis, suggesting that TAD-modification does not endow the LNP with additional membrane destabilizing properties (**Figure S22).** To assess whether TAD-conjugation of PEG-DMG alters the colloidal stability of LNP in serum, we incubated LNP formulations in 10% serum at 37°C, followed by analysis via asymmetric field flow fractionation-multi angle light scattering (AFFF-MALS). We found that all LNPs increased in size, likely due to protein adsorption onto their surface, but remained stable for up to at least 3 days as no signs of aggregate formation emerged in the elugrams depicted in **Figure S23**. The underlying reason for the enhanced transfection efficiency of TAD-PEG-DMG LNP therefore remains elusive and will be subject of future studies. Notwithstanding, our results highlight the potential of a rather simple, one-step modification on the PEG backbone to improve the transfection efficiency of mRNA LNP *in vitro*.

In Vivo mRNA Transfection Efficiency of TAD-PEG-lipid LNP

Transfection efficiency *in vivo*, in mice, was evaluated using mRNA encoding for firefly luciferase (Fluc), as a reporter protein, in combination with Cy7-1,2-distearoyl-sn-glycero-3-phosphoethanolamine (DSPE-Cy7) labeled LNP for concomitant bioluminescence imaging of the luciferase expression and tissue distribution of LNP. Balb/c mice received a 5 µg mRNA dose by intravenous injection into tail vein. 4 h and 24 h post injection luciferase expression was measured by bioluminescence imaging. After the 24 h time point, the major organs were dissected, and their bioluminescence was measured. The photon flux was measured for quantification of the Fluc expression level. ^{Butyl}TAD-PEG-DMG LNP induced a Fluc expression lower than PEG-DMG LNP, both on the level of the whole-body Fluc expression (**Figure 6A**) as well as on the tissue level in liver and spleen (**Figure 6B**). Fluc expression and Cy7 fluorescence showed similar profiles, indicating that protein, *i.e.*, Fluc, was effectively produced in those tissues where LNPs accumulated (**Figure 6B-C**). Predictably, ^{HexanoicAcid}TAD-PEG-DMG LNPs induced negligeable luciferase expression and tissue accumulation (**Figure S24**) likely due to their large size (*vide supra*).[39] Several recent studies reported on the impact of the surface charge of LNPs on their biodistribution, with the ability to target different tissues.[41,43,44] This was not observed in our case. TAD modification could also alter the protein corona of the LNP which is known to impact cellular interaction. In particular, the influence of TAD-modification on the adsorption of apolipoprotein E, which mediates uptake of LNP by hepatocytes in the liver, might be of relevance and merits attention in future studies.[45] On the one hand, it should be noted that PEG-DMG is quickly released from the surface of LNP and replaced by serum proteins.[46] Hence, it is likely to assume that the longevity of ^{Butyl}TAD-PEG-DMG on the LNP surface was insufficient to alter the pharmacokinetic profile of the LNP and to augment mRNA transfection upon cellular uptake, as was observed *in vitro*. On the other hand, the slightly larger size of ^{Butyl}TAD-PEG-DMG compared to PEG-DMG LNP could potentially also have altered the pharmacokinetic profile, as overall deposition of ^{Butyl}TAD-PEG-DMG LNP in liver and spleen was lower.

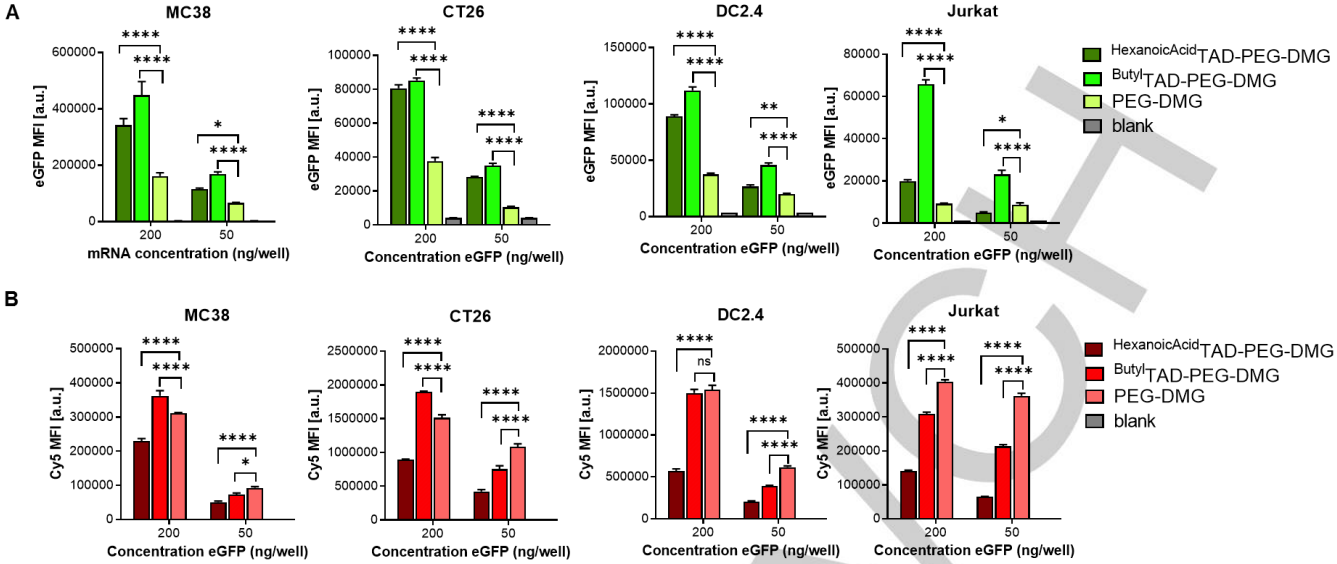

Figure 5. Flow cytometry analysis of (**A**) eGFP expression and (**B**) cellular uptake of LNPs stabilized by TAD-modified and unmodified PEG-lipids on different cell lines (i.e. murine colon adenocarcinoma, MC38; murine colorectal carcinoma, CT26; murine dendritic cells, DC2.4; and human T lymphocytes, Jurkat). Data are presented as the median fluorescence of 3 experimental repeats ± standard deviation. Statistical significance was calculated with two-way ANOVA with multiple comparisons (ns: non-significant; *p < 0.05; **p < 0.01; ***p < 0.001).

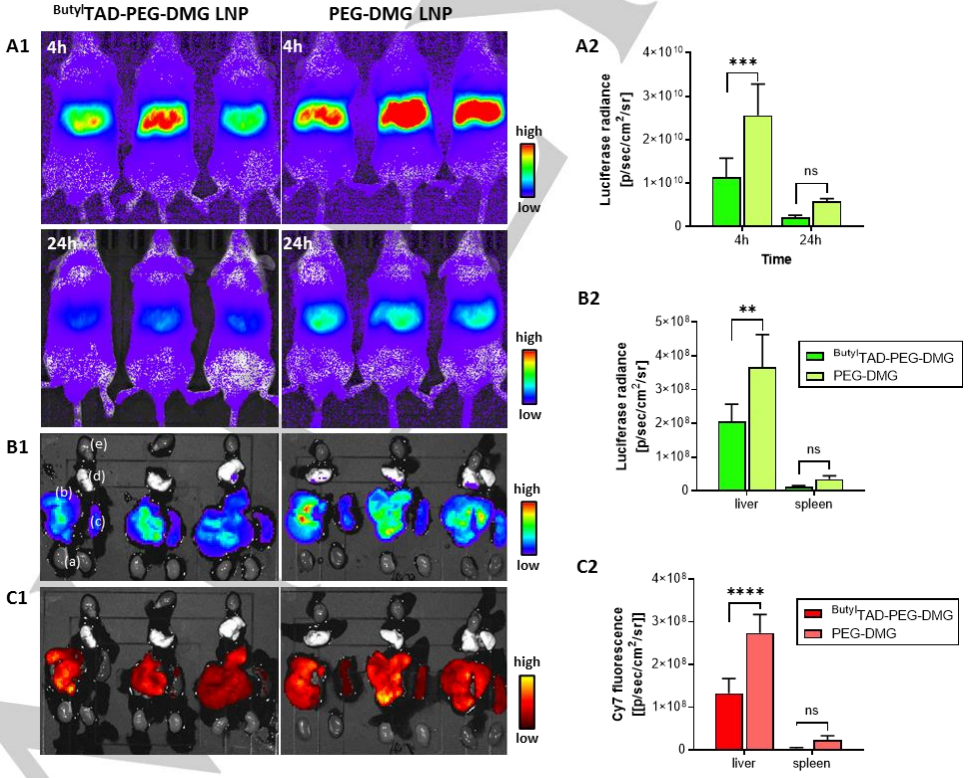

Figure 6. (**A**) *In vivo* bioluminescence after 4h and after 24h post intravenous administration of LNP: (**A1**) Bioluminescence imaging. (**A2**) Quantification of luciferase expression by measurement of the photon flux. (**B**) Luciferase expression in dissected tissues after 24 h. (**B1**) Bioluminescence imaging (a: kidneys, b: liver, c: spleen, d: lungs, e: heart). (**B2**) Quantification of luciferase expression by measurement of the photon flux. (**C**) Tissue distribution of the Cy7 signal after 24h. (**C1**) Fluorescence imaging. (**C2**) Quantification of the fluorescent signal. Data are presented as the mean luciferase radiance (or Cy7 fluorescence) ± standard deviation, n = 3. Statistical significance was calculated with one-way ANOVA with multiple comparisons (ns: non-significant; *p < 0.05; **p < 0.01; ***p < 0.001).

Conclusion

In conclusion, we have demonstrated that photo-modification of PEG and PEG-lipid with hexanoic acid and butyl TAD derivatives concomitantly introduces functionality and degradability along the PEG backbone. Hydrolysis kinetics of TAD-PEG and TAD-PEG-lipid were dependent on pH and temperature of the aqueous environment and were also slightly influenced by the nature of the TAD substituent. TAD-PEG-lipid LNPs could efficiently encapsulate mRNA into LNP without impacting LNP stability. However, only ^{Butyl}TAD-PEG-DMG afforded sub 150 nm sized LNPs. *In vitro*, on multiple cell lines, TAD-PEG-DMG formulated mRNA LNPs showed higher transfection efficiency than common PEG-DMG LNPs. Furthermore, TAD-modified LNPs were non-toxic within the tested concentration range *in vitro*. Finally, *in vivo* studies in mice of ^{Butyl}TAD-PEG-DMG formulated mRNA LNPs showed a similar biodistribution, with predominant targeting of liver and spleen, similar to common PEG-DMG LNP, with the overall transfection efficacy only being slightly lower.

Our herein presented findings provide a first glimpse of TAD-modified PEGs to provide a powerful strategy in a nanomedicine context. Our initial study highlights many promising aspects that merit further investigation, including (1) the exact role of the TAD derivatives on improving *in vitro* mRNA transfection, (2) whether the use of longer alkyl PEG-lipids that have greater longevity on the LNP surface might have a more profound effect on the biodistribution of LNPs *in vivo*, (3) whether the degree of substitution can be altered to tune the rate of overall degradation, (4) whether specific functionalities can be introduced on commercial PEGs to exploit other purposes, by using TAD compounds bearing, e.g., a fluorescent tracer or targeting ligand, and (5) whether the inherent degradability of TAD-PEG can be leveraged to mitigate PEG-related side-effects of nanomedicines or protein conjugates.

Acknowledgements

BGDG acknowledges the FWO Flanders for funding (grant °N G019819N). BGDG and FEDP acknowledge Ghent University for funding (BOF-GOA).

Conflict of Interest

The authors declare no conflict of interest.

Keywords: lipid nanoparticles • mRNA • drug delivery • degradable PEG • multifunctional PEG

[1] U. Sahin, K. Karikó, Ö. Türeci, *Nat. Rev. Drug Discov.* **2014**, *13*, 759–780.

[2] N. Pardi, M. J. Hogan, F. W. Porter, D. Weissman, *Nat. Publ. Gr.* **2018**, *17*, 261–279.

[3] A. Wadhwa, A. Aljabbari, A. Lokras, C. Foged, A. Thakur, *Pharmaceutics* **2020**, *12*, 102.

[4] X. Hou, T. Zaks, R. Langer, Y. Dong, *Nat. Rev. Mater.* **2021**, *6*, 1078–1094.

[5] K. L. Swingle, A. G. Hamilton, M. J. Mitchell, *Trends Mol. Med.* **2021**, *27*, 616–617.

[6] S. H. Kiaie, N. Majidi Zolbanin, A. Ahmadi, R. Bagherifar, H. Valizadeh, F. Kashanchi, R. Jafari, *J. Nanobiotechnology* **2022**, *20*, 1–20.

[7] C. Hald, J. A. Kulkarni, D. Witzigmann, M. Lind, K. Petersson, J. B. Simonsen, *Adv. Drug Deliv. Rev.* **2022**, *188*, 114416.

[8] Y. Zhang, C. Sun, C. Wang, K. E. Jankovic, Y. Dong, **2021**, *121*, 12181-12277.

[9] Z. Hussain, S. Khan, M. Imran, M. Sohail, S. W. A. Shah, M. de Matas, *Drug Deliv. Transl. Res.* **2019**, *9*, 721–734.

[10] P. E. Lipsky, L. H. Calabrese, A. Kavanaugh, J. S. Sundy, D. Wright, M. Wolfson, M. A. Becker, *Arthritis Res. Ther.* **2014**, *16*, 1–8.

[11] Y. Mima, Y. Hashimoto, T. Shimizu, H. Kiwada, T. Ishida, *Mol. Pharm.* **2015**, *12*, 2429–2435.

[12] A. S. A. Lila, M. Ichihara, T. Shimizu, T. Ishida, H. Kiwada, *Biol. Pharm. Bull.* **2013**, *36*, 1842–1848.

[13] T. Ishida, M. Ichihara, X. Y. Wang, H. Kiwada, *J. Control. Release* **2006**, *115*, 243–250.

[14] X. Y. Wang, T. Ishida, H. Kiwada, *J. Control. Release* **2007**, *119*, 236–244.

[15] Y. Hashimoto, Y. Uehara, A. S. Abu Lila, T. Ishida, H. Kiwada, *Gene Ther.* **2014**, *21*, 593–598.

[16] Y. Ju, J. M. Carreño, V. Simon, K. Dawson, F. Krammer, S. J. Kent, *Nat. Rev. Immunol.* **2022**, *23*, 135–136 .

[17] S. S. Nogueira, A. Schlegel, K. Maxeiner, B. Weber, M. Barz, M. A. Schroer, C. E. Blanchet, D. I. Svergun, S. Ramishetti, D. Peer, P. Langguth, U. Sahin, H. Haas, *ACS Appl. Nano Mater.* **2020**, *3*, 10634–10645.

[18] K. Knop, R. Hoogenboom, D. Fischer, U. S. Schubert, *Angew. Chemie - Int. Ed.* **2010**, *49*, 6288–6308.

[19] X. Zhu, W. Tao, D. Liu, J. Wu, Z. Guo, X. Ji, Z. Bharwani, L. Zhao, X. Zhao, O. C. Farokhzad, J. Shi, *Theranostics* **2017**, *7*, 1990–2002.

[20] G. F. Walker, C. Fella, J. Pelisek, J. Fahrmeir, S. Boeckle, M. Ogris, E. Wagner, *Mol. Ther.* **2005**, *11*, 418–425.

[21] M. Niu, Y. W. Naguib, A. M. Aldayel, Y. C. Shi, S. D. Hursting, M. A. Hersh, Z. Cui, *Mol. Pharm.* **2014**, *11*, 4425–4436.

[22] J. Cui, R. De Rose, K. Alt, S. Alcantara, B. M. Paterson, K. Liang, M. Hu, J. J. Richardson, Y. Yan, C. M. Jeffery, R. I. Price, K. Peter, C. E. Hagemeyer, P. S. Donnelly, S. J. Kent, F. Caruso, *ACS Nano* **2015**, *9*, 1571–1580.

[23] Y. Tian, Z. Gao, N. Wang, M. Hu, Y. Ju, Q. Li, F. Caruso, J. Hao, J. Cui, *J. Am. Chem. Soc.* **2022**, *144*, 18419–18428.

[24] J. Blankenburg, K. Maciol, C. Hahn, H. Frey, *Macromolecules* **2019**, *52*, 1785–1793.

[25] O. Linker, J. Blankenburg, K. Maciol, M. Bros, H. Frey, *Macromolecules* **2020**, *53*, 3524–3534.

[26] T. Johann, H. A. Houck, T. Dinh, U. Kemmer-Jonas, F. E. Du Prez, H. Frey, *Polym. Chem.* **2019**, *10*, 4699–4708.

[27] H. A. Houck, P. Müller, M. Wegener, C. Barner-Kowollik, F. E. Du Prez, E. Blasco, *Adv. Mater.* **2020**, *32*, 2003060.

[28] F. Risi, A. M. Alstanei, E. Volanschi, M. Carles, L. Pizzala, J. P. Aycard, *European J. Org. Chem.* **2000**, 617–626.

[29] T. Yamaoka, Y. Tabata, Y. Ikada, *J. Pharm. Sci.* **1994**, *83*, 601–606.

[30] B. Liu, S. Thayumanavan, *J. Am. Chem. Soc.* **2017**, *139*, 2306–2317.

[31] P. Phoungtawee, F. Seidi, A. Treetong, C. Warin, A. Klamchuen, D. Crespy, *ACS Macro Lett.* **2021**, *10*, 365–369.

[32] F. Seidi, V. Druet, N. Huynh, T. Phakkeeree, D. Crespy, *Chem. Commun.* **2018**, *54*, 13730–13733.

[33] R. C. Cookson, I. D. R. Stevens, C. T. Watts, *Chem. Commun.* **1965**, 259–260.

[34] N. Dararatana, F. Seidi, D. Crespy, *Polymer (Guildf).* **2020**, *194*, 122346.

[35] K. De Bruycker, S. Billiet, H. A. Houck, S. Chattopadhyay, J. M. Winne, F. E. Du Prez, *Chem. Rev.* **2016**, *116*, 3919–3974.

[36] S. B. Hanay, A. Fallah, E. Senturk, Z. Yetim, F. Afghah, H. Yilmaz, M. Culha, B. Koc, A. Zarrabi, R. S. Varma, *Gels* **2021**, *7*, 261.

[37] M. J. Bausch, B. David, P. Dobrowolski, R. Gostowski, D. Selmarten, V. Prasad, A. Vaughn, L. Wang, **1991**, 5643–5651.

[38] M. J. Carrasco, S. Alishetty, M. G. Alameh, H. Said, L. Wright, M. Paige, O. Soliman, D. Weissman, T. E. Cleveland, A. Grishaev, M. D. Buschmann, *Commun. Biol.* **2021**, *4*, 1–15.

[39] E. Samaridou, J. Heyes, P. Lutwyche, *Adv. Drug Deliv. Rev.* **2020**, *154–155*, 37–63.

[40] B. Bogaert, F. Sauvage, R. Guagliardo, C. Muntean, V. P. Nguyen, E. Pottie, M. Wels, A. K. Minnaert, R. De Rycke, Q. Yang, D. Peer, N. Sanders, K. Remaut, Y. M. Paulus, C. Stove, S. C. De Smedt, K. Raemdonck, *J. Control. Release* **2022**, *350*, 256–270.

[41] R. Pattipeiluhu, G. Arias-Alpizar, G. Basha, K. Y. T. Chan, J. Bussmann, T. H. Sharp, M. A. Moradi, N. Sommerdijk, E. N. Harris, P. R. Cullis, A. Kros, D. Witzigmann, F. Campbell, *Adv. Mater.* **2022**, *34*, 2201095.

[42] M. Maugeri, M. Nawaz, A. Papadimitriou, A. Angerfors, A. Camponeschi, M. Na, M. Hölttä, P. Skantze, S. Johansson, M. Sundqvist, J. Lindquist, T. Kjellman, I. L. Mårtensson, T. Jin, P. Sunnerhagen, S. Östman, L. Lindfors, H. Valadi, *Nat. Commun.* **2019**, *10*, 4333.

[43] S. T. LoPresti, M. L. Arral, N. Chaudhary, K. A. Whitehead, *J. Control. Release* **2022**, *345*, 819–831.

[44] Q. Cheng, T. Wei, L. Farbiak, L. T. Johnson, S. A. Dilliard, D. J. Siegwart, *Nat. Nanotechnol.* **2020**, *15*, 313–320.

[45] A. Akinc, W. Querbes, S. De, J. Qin, M. Frank-kamenetsky, K. N. Jayaprakash, M. Jayaraman, K. G. Rajeev, W. L. Cantley, J. R. Dorkin, J. S. Butler, L. Qin, T. Racie, A. Sprague, E. Fava, A. Zeigerer, M. J. Hope, M. Zerial, D. W. Y. Sah, K. Fitzgerald, M. A. Tracy, M. Manoharan, V. Koteliansky, A. De Fougerolles, M. A. Maier, *Mol. Ther.* **2009**, *18*, 1357–1364.

[46] B. L. Mui, Y. K. Tam, M. Jayaraman, S. M. Ansell, X. Du, Y. Y. C. Tam, P. J. Lin, S. Chen, J. K. Narayanannair, K. G. Rajeev, M. Manoharan, A. Akinc, M. A. Maier, P. Cullis, T. D. Madden, M. J. Hope, *Mol. Ther. - Nucleic Acids* **2013**, *2*, e139.

Entry for the Table of Contents

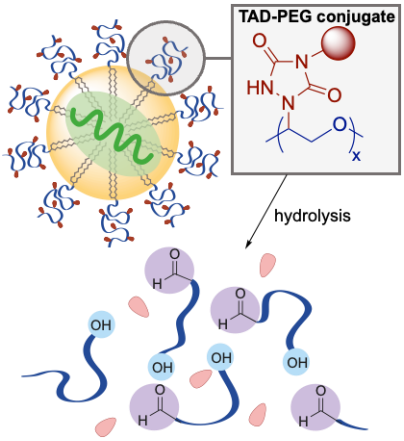

TOC text: Conjugation of triazolinediones to poly(ethylene glycol) under visible light irradiation, introduces labile bonds into the polymer backbone. These polymers can be used for engineering mRNA lipid nanoparticle formulations with a polymer coating that is degradable under physiologically relevant aqueous conditions.